

Silver Nanoparticle-Loaded Contact Lenses for Blue-Yellow Color Vision Deficiency

Ahmed E. Salih,* Aya Shanti, Mohamed Elsherif, Fahad Alam, Sungmun Lee, Kyriaki Polychronopoulou, Fahad Almaskari, Habiba AlSafar, Ali K. Yetisen, and Haider Butt*

Contact lenses can be functionalized to offer advanced capabilities transcending their primary applications in vision correction and cosmetics. Herein, 40 and 60 nm spherical silver nanoparticles (SNPs) are integrated within poly(2-hydroxyethyl methacrylate) (pHEMA) contact lenses toward fabrication of SNP-loaded contact lenses with excellent optical and material properties as wearables for blue-yellow color vision deficiency (CVD) patients. The morphology and optical properties of the SNPs are characterized prepolymerization using the transmission electron microscopy (TEM) and an optical spectrophotometer. Then, the transmission spectra of the SNP-loaded contact lenses at different concentrations along with the wettability and water content are measured, to demonstrate the effect of NPs' addition on the lenses' optical and material characteristics. Results indicate that the transmission spectra of SNP-loaded contact lenses, with optimum concentrations, filter out problematic wavelengths of visible light (485–495 nm), which will facilitate better color distinction for blue-yellow CVD patients. The contact lenses' optical properties are analogous to the commercial colorblind glasses, indicating their effectiveness as color filtering wearables. Finally, the cytobiocompatibility analysis of the contact lenses to RAW 264.7 culture of cells shows that they are biocompatible, and the cell viability remains higher than 75% after 24 h in contact with the lenses.

1. Introduction


1.1. Silver Nanoparticles: Properties and Optical Applications

Silver nanoparticles (SNPs) have been extensively utilized in biomedical related applications, which include sensing, drug delivery, cancer therapy, X-ray imaging, and optical processes.^[1] SNPs are particularly attractive for the aforementioned applications as they are biocompatible and both chemically and physically stable. Moreover, SNPs are highly effective in absorbing and scattering light, and their surface plasmon resonance (SPR) is responsible for this optical behavior. SPR refers to the collective oscillation of conduction electrons due to the electromagnetic field of the incident light and occurs as a result of the motion of the NPs' conduction electrons.^[1–3] The SPR band of SNPs relies primarily on their morphology (e.g., shape, size) and can be tuned by adjusting parameters affecting the morphology/medium (e.g., solvent).^[4] Further, the extinction,

absorption, and scattering of NPs are explained by the Mie theory.^[5] The Mie theory is an analytical solution to the

A. E. Salih, M. Elsherif, F. Alam, K. Polychronopoulou, H. Butt
Department of Mechanical Engineering
Khalifa University
Abu Dhabi P.O. Box 127788, UAE
E-mail: aesarli95@gmail.com; haider.butt@ku.ac.ae

A. Shanti, S. Lee
Department of Biomedical Engineering and Healthcare Engineering
Innovation Center
Khalifa University
Abu Dhabi P.O. Box 127788, UAE

 The ORCID identification number(s) for the author(s) of this article can be found under <https://doi.org/10.1002/pssa.202100294>.

© 2021 The Authors. physica status solidi (a) applications and materials science published by Wiley-VCH GmbH. This is an open access article under the terms of the Creative Commons Attribution License, which permits use, distribution and reproduction in any medium, provided the original work is properly cited.

DOI: 10.1002/pssa.202100294

F. Almaskari
Department of Aerospace Engineering
Khalifa University
Abu Dhabi P.O. Box 127788, UAE

H. AlSafar
Department of Biomedical Engineering
Khalifa University
Abu Dhabi P.O. Box 127788, UAE

H. AlSafar
Centre for Biotechnology
Khalifa University
Abu Dhabi P.O. Box 127788, UAE

H. AlSafar
Department of Genetics and Molecular Biology
College of Medicine and Health Sciences
Khalifa University
Abu Dhabi P.O. Box 127788, UAE

Maxwell's equations, and it explains the extinction caused by scattering and absorption behaviors of the NPs. The extinction, absorption, and scattering equations are provided in Equation (1)–(7).^[6]

$$\sigma_{\text{ext}} = \frac{2\pi}{k^2} \sum_{j=1}^{\infty} (2j+1) \text{Re}(a_j + b_j) \quad (1)$$

$$\sigma_{\text{sca}} = \frac{2\pi}{k^2} \sum_{j=1}^{\infty} (2j+1) (|a_j|^2 + |b_j|^2) \quad (2)$$

$$\sigma_{\text{abs}} = \sigma_{\text{ext}} - \sigma_{\text{sca}} \quad (3)$$

$$a_j = \frac{\frac{n}{n_m} \psi_j(\frac{n}{n_m} |k|R) \psi'_j(|k|R) - \psi_j(|k|R) \psi'_j(\frac{n}{n_m} |k|R)}{\frac{n}{n_m} \psi_j(\frac{n}{n_m} |k|R) \zeta'_j(|k|R) - \zeta_j(|k|R) \psi'_j(\frac{n}{n_m} |k|R)} \quad (4)$$

$$b_j = \frac{\psi_j(\frac{n}{n_m} |k|R) \psi'_j(|k|R) - \frac{n}{n_m} \psi_j(|k|R) \psi'_j(\frac{n}{n_m} |k|R)}{\psi_j(\frac{n}{n_m} |k|R) \zeta'_j(|k|R) - \frac{n}{n_m} \zeta_j(|k|R) \psi'_j(\frac{n}{n_m} |k|R)} \quad (5)$$

where n , R , n_m , and k represent the refractive index (RI) and radius of the NP, RI of the medium, and wavelength of incident light, respectively. ψ_j and ζ_j are the Riccati–Bessel functions, and they are given as follows

$$\psi_j(x) = \sqrt{\frac{\pi x}{2}} J_{j+\frac{1}{2}}(x) \quad (6)$$

$$\zeta_j(x) = \sqrt{\frac{\pi x}{2}} [J_{j+\frac{1}{2}}(x) + iY_{j+\frac{1}{2}}(x)] \quad (7)$$

where J_ν and Y_ν are the Bessel functions of the first and second order, respectively. The RI of the NPs' medium and the size of the NPs are the main parameters affecting their scattering and absorption profiles. Although the theory does not account for the particles' interactions among themselves which might induce aggregation or agglomeration, it provides an adequate prediction for the absorption/transmission spectrum of the NPs at a given size and in a medium of a specific RI. Moreover, absorption dominates in NPs that are relatively smaller than the wavelength of the incident light (less than 100 nm) whereas for NPs that are comparable to the wavelength of light, the scattering effects prevail.^[7,8] The ability to tune the absorption and scattering of the NPs makes them useful for applications such as biomedicine,^[9] energy,^[10] and electronics.^[11]

Furthermore, due to their superior optical properties, SNPs were added to different polymers, thus forming silver nanocomposites (SNCs) targeted for various ocular applications.^[12–14] Prosycevas et al. incorporated SNPs into polymethylmethacrylate–polyethylene terephthalate (PMMA–PET) by electron beam evaporation.^[15] The SPR of the NPs was evident in the developed silver–polymer nanocomposites, indicating successful coating. The SPR varied from 425 to 600 nm depending on the layer thickness of the coating. The formed composites showed adequate properties and looked promising for manufacturing ultrathin

color filters.^[15] López et al. embedded SNPs into polyvinyl alcohol (PVA) by using a Microplotter and then thermally polymerized the solution.^[16] The fabricated nanocomposite showed excellent sensing properties through identifying chicken meat spoilage. The main principle involved the color change of the nanocomposite; when it changed from yellow to colorless, the chicken was probably spoiled due to the release of volatile compounds. Authors reported that this could be a basis for smart packaging technologies.^[16] Additionally, Forrest et al. reported the doping of contact lenses with SNPs to aid patients suffering from retinal or ocular disorders, which may hinder some of their day-to-day activities, especially in bright light environments.^[17] The latter was one of the prominent examples of contact lenses' utilization for the treatment of ocular deficiencies. Indeed, the need for continuous health monitoring through noninvasive techniques has paved the way for the incorporation of various physical and chemical biomarkers into contact lenses for the diagnosis and treatment of diseases such as glaucoma, dry eye, AIDS, and diabetes.^[18] Moreover, several studies not only examined the detection of such diseases but also developed methods to real-time monitor and report, through smart phones, any abnormalities in the levels of these diseases.^[19,20] For instance, Ku et al. developed a novel smart contact lens system by integrating sensors, wireless antennas, and electric components into a soft contact lens for the detection of cortisol levels through eye tears.^[20] A near-field communication (NFC) chip was also incorporated into the lens to allow for real-time transmission of the data to the user's smart phone. Trials on humans and in vivo tests on live rabbits ensured the biocompatibility and potential efficacy of this smart lens as a noninvasive mobile health care solution that provides clinical information.^[20]

1.2. Incorporation of NPs into Contact Lenses for Color Blindness Management

1.2.1. Color Vision Deficiency: Types and Prominence

More recently, Salih et al. incorporated gold (Au) NPs into contact lenses to enhance color distinction for red-green colorblind patients.^[21] Color blindness or color vision deficiency (CVD) is a congenital disorder, which hinders patients from distinguishing certain colors. Congenital CVD is inherited in the X chromosome and affects 8% of males and 0.5% of females.^[22–24] Most colorblind patients have either a defective or a missing photoreceptor cone cell, which causes the loss in sensitivity of some colors. There are three types of photoreceptors cone cells which facilitate color vision: short (S) cones, medium (M) cones, and long (L) cones; those are also commonly referred to as blue, green, and red cells, respectively.^[25] Further, there are three different forms of color blindness, depending on the conditions of each photoreceptor: anomalous trichromacy (defective cone), dichromacy (single missing cone), and monochromacy (missing at least two cones). Almost 95% of all CVD patients suffer from red-green colorblindness, in which the M and L cones are

A. K. Yetisen
Department of Chemical Engineering
Imperial College London
London SW7 2AZ, UK

H. Butt
School of Engineering
University of Birmingham
Birmingham B15 2TT, UK

missing or faulty whereas others, who have a missing or faulty S cone, are regarded as blue-yellow colorblind patients.

1.2.2. Ophthalmic Wearable Aids for CVD Patients

Further, the lenses developed by Salih et al. were the first in which the addition of gold NPs to hydrogel materials was targeted for CVD application.^[21] However, ophthalmic wearables, which utilize dyed customized filters to alter the wavelength of the colors perceived by the patients' eyes, have recently gained massive attention.^[21,25–29] These wearables operate on a principle, introduced by Seebeck,^[30] who noted that patients' photoreceptor cones are simulated individually rather than simultaneously when they look through a red and green filter, consecutively. Utilizing the latter concept, companies manufactured glasses and contact lenses as wearable aids for CVD patients. One of the most prominent CVD glasses is developed by Enchroma, which has experimentally shown its efficacy in enhancing color distinction and perception for color blind patients. These glasses are customized as per the patient's CVD type, but they generally filter out common problematic wavelengths from the visible light spectrum, which occur at 520–580 nm (for red-green crossover) and 450–500 nm (for blue-green crossover).^[31] Moreover, companies such as Colormax and Chromagen used the same concept of colored filters to fabricate contact lenses that enhance color distinction for CVD patients. Also, Badawy et al. used Atto dyes to fabricate rose tinted contact lenses, which the authors tested on patients and reported their high effectiveness.^[26]

1.2.3. SNP-Loaded Contact Lenses

Nonetheless, nearly all contact lenses established by CVD companies and researchers target red-green CVD with little emphasis on blue-yellow color blindness as it is less prominent. The combination of these colored filters blocks out the M–L cones' overlapping wavelengths (520–580 nm), which is ideal for patients suffering from red-green color blindness.^[25] However, for blue-yellow CVD patients, several studies showed that filtering should occur at the S–M–L crossover range (450–500 nm).^[32] As outlined earlier, spherical SNPs absorb visible light in the range of 390–490 nm depending on their size and their dielectric medium. Utilizing their effectiveness in absorbing light in the aforementioned ranges and their high biocompatibility, we integrated SNPs with distinct sizes into contact lenses to alleviate color distinction for blue-yellow CVD patients. The optical performance of these lenses was evaluated against other CVD wearables such as Enchroma, to determine their efficacy. To the best of our knowledge, no prior studies have assessed SNP-loaded contact lenses as wearable aids for blue-yellow CVD patients.

2. Experimental Section

2.1. Chemicals

2-Hydroxyethyl methacrylate (HEMA, 97%) containing ≤ 250 ppm of monomethyl ether hydroquinone as inhibitor,

ethylene glycol dimethacrylate (EGDMA, 98%) containing 90–110 ppm of monomethyl ether hydroquinone as inhibitor, and 2-hydroxy-2-methylpropiophenone (97%) were purchased and used from Sigma-Aldrich as is without further purification. SNPs (40 and 60 nm) (Cat No. 730807 and 730815) dispersed in aqueous buffer with concentration of 0.02 mg mL^{-1} were also obtained from Sigma-Aldrich.

2.2. Cell Culture

Raw 264.7 (ATCC, Manassas, VA, USA) cells were cultured in Dulbecco's Modified Eagle Medium (DMEM) containing 4.5 g L^{-1} D-glucose, 0.584 g L^{-1} L-glutamine, and 0.11 g L^{-1} sodium pyruvate (Gibco, Fisher Scientific, Waltham, MA, USA). The media was supplemented with 10% fetal bovine serum (FBS) (Gibco) and 1% penicillin–streptomycin (Gibco). The cells were incubated at 37°C and 5% CO_2 .

2.3. Fabrication

The SNP-loaded contact lenses were fabricated by first mixing 1.5 mL of HEMA, 10 μL of EGDMA, and 5 μL of 2-hydroxy-2-methylpropiophenone (photoinitiator) and then adding the solution to a glass cuvette which was left to sonicate for 30 min to ensure complete homogenization. Then, depending on the required concentration of the NPs, a specific volume of the solution was centrifuged, and the resulting volume was used in the hydrogel solution. After that, the solution was again sonicated for 30 min, and 110 μL of the solution was added to the contact lens mold. It was then polymerized through a 365 nm wavelength UV lamp for 5–10 min. The formed gel was then washed using deionized (DI) water. The synthesis process is illustrated in **Figure 1a**. The concentrations of the NPs within the SNP-loaded contact lenses were optimized after many trials to get the best possible material and optical properties. In fact, four concentrations per each utilized set of NPs were added to the hydrogel prior to polymerizing it. The latter was done to show the effect of the concentrations on the properties of the SNP-loaded contact lenses. For the 40 nm set, the added concentrations were 0.67, 1, 1.33, and 1.67% v/v of the hydrogel solution. Likewise, for the 60 nm set, the used concentrations were 0.33, 0.67, 1.33, and 1.67% v/v. These concentrations were added from the volume, resulting from centrifuging 3 mL of the parent NP. The fabrication process was performed at ambient conditions.

2.4. Prepolymerization Characterization

The experimental procedure in conducting the prepolymerization characterization which includes UV–vis spectroscopy, morphology imaging using transmission electron microscopy (TEM), and RI measurements is detailed in this subsection.

Optical: The transmission spectrum of the NPs' solution was obtained using a UV–vis spectrophotometer connected to an optical microscope. The spectrophotometer used was USB 2000+ provided by Ocean Optics which operates in the range of 200–1100 nm. Furthermore, the NPs' solution was characterized by depositing 500 μL of it into a cuvette and recording the transmission/absorption spectrum using OceanView software.

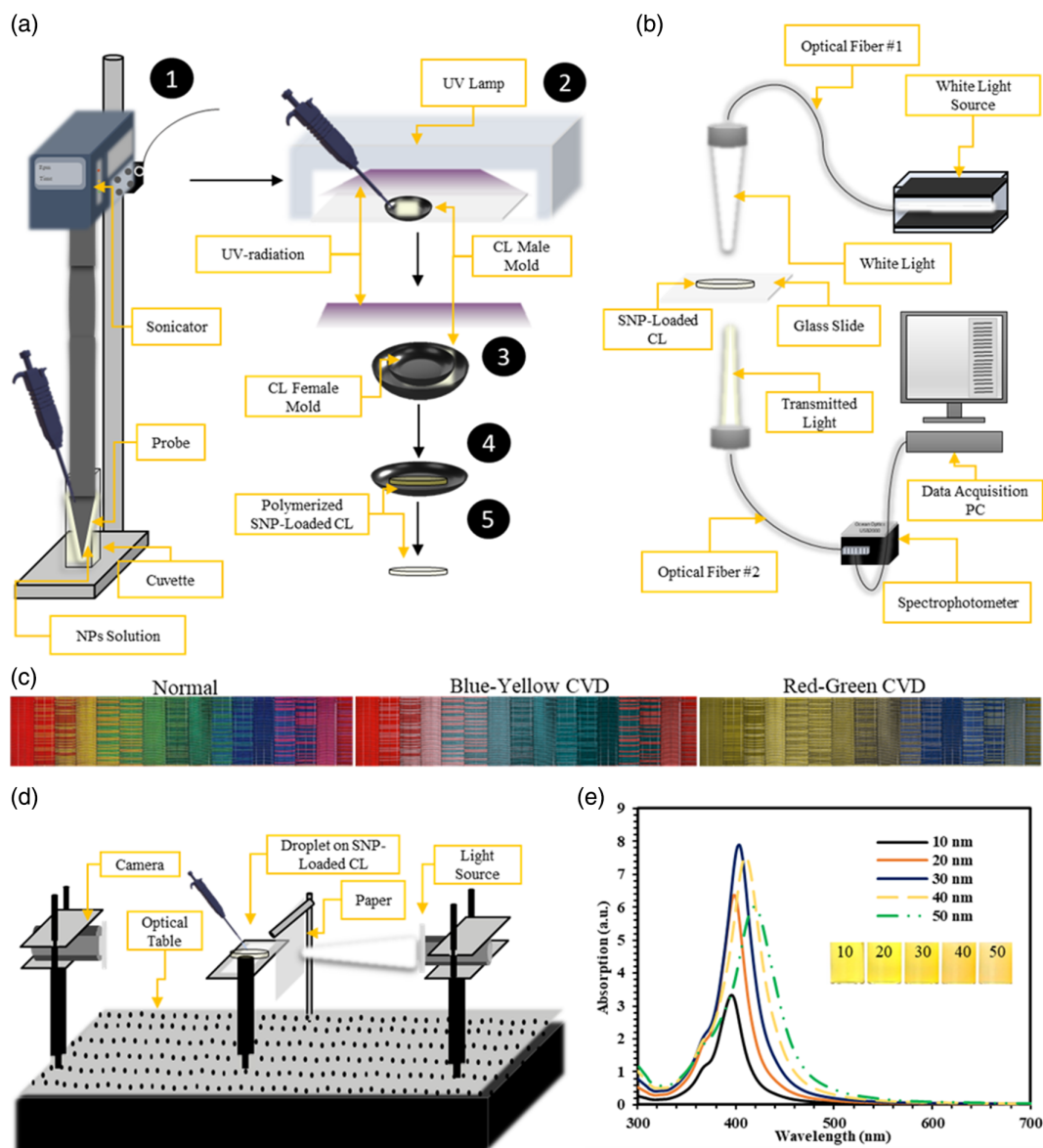


Figure 1. Fabrication and characterization of SNP-loaded contact lenses (CL) for blue-yellow CVD: a) steps for synthesizing the lenses; b) schematic of the transmission spectroscopy measurement; c) visual perception of colors by normal individuals and CVD patients; d) schematic of the contact angle measurement setup; and e) absorption spectra of SNPs with various sizes at a RI of 1.33 using a Mie theory code adapted from C. F. Bohren and D. R. Huffman.

Further, the RI of the NPs' medium effect on the transmission/absorption spectrum was examined, as previous studies showed that NPs' optical properties heavily depend on the dielectric media of the NPs.^[33] The RI of the NPs' medium was measured by adding 50 μL of the NPs' solution to the glass of a handheld refractometer (KERN ORA-B). HEMA (RI:1.453) and water (RI:1.33) were used to vary the RI of the NPs' medium. These measurements were evaluated against theoretical predictions from the Mie theory. To simulate the response of the SNPs in various mediums, a MATLAB code adapted from C. F. Bohren and D. R. Huffman was utilized.^[6]

Morphology: Tecnai TEM 200 kV was used to obtain information on the NPs, particularly their morphology. Copper mesh

grids provided by TED PELLA were used. Moreover, 10 μL of the NPs solution was dispersed on the grid and kept in a vacuum oven for 2 h at 50 $^{\circ}\text{C}$ to dry. The grids were removed, and the same procedure was done three times to get as much NPs as possible in the grid. Resulting images were processed using ImageJ software.

2.5. Postpolymerization Characterization

The postpolymerization characterization is provided in this subsection and includes micrographs of the cross section, transmission spectrum, water content, and wettability properties of the nanocomposite material.

Optical: Transmission spectrum of the SNP-loaded contact lens was measured using the same steps outlined earlier and summarized in Figure 1b.

Physiochemical: After that, the water content was measured. For that, the lens was first placed in a vacuum oven at 40 °C for 6 h whereby its moisture was removed; subsequently, the corresponding dry mass was measured. The SNP-loaded contact lens was then immersed in 5 mL of DI water and left to swell until no further change in its total mass was noted. The minimum number of hours needed to ensure complete water retention of the lens was 72 h. Moreover, the wettability of the lens was determined by measuring its contact angle using the sessile drop method.^[34] A schematic of the experimental setup of the contact angle measurement is shown in Figure 1d. Moreover, 5 μ L of DI water was dropped on the SNP-loaded contact lens, and the contact angle of the droplet on the surface was directly captured. The image was analyzed, and the contact angle was measured using ImageJ software.

Morphology: Then, to obtain the morphology of the NPs within the lens, scanning electron microscope (SEM) was used. The SNP-loaded contact lenses were sheared after being dried again, and their cross sections were imaged. Two SNP-loaded contact lenses, which had the lowest and highest concentrations, per set were characterized using the SEM.

Cytobiocompatibility: Finally, to measure the cytobiocompatibility of lenses, MTT (3-(4,5-dimethylthiazol-2-yl)-2,5-diphenyl-tetrazolium bromide) reduction assay was performed using RAW 264.7 cells as model cells. Cells were seeded in 12 well plates at a concentration of 5×10^5 cells mL⁻¹ and incubated for 24 h at 37 °C and 5% CO₂. After 24 h, lenses washed twice in serum-free medium were added to the cells. The cells were then incubated for an additional 24 h. After 24 h, the lenses were removed from

the wells and MTT was added to the cells. The cells were subsequently incubated for 4 h. During the incubation time, yellow MTT solution was reduced to purple formazan in living cells. After 4 h, media containing MTT was removed and replaced by dimethyl sulfoxide (DMSO) to dissolve the formazan crystals. Next, the absorbance of each sample was measured at 570 nm using a microplate reader. Percentage cell viability was calculated by comparing the absorbance of the control cells (cells with medium only and no lens) to that of cells with the lenses, as per the below ratio:

$$\text{Percentage cell viability} = (\text{cells with lens and MTT}) / (\text{control cells with MTT but no lens}) \times 100.$$

3. Results and Discussion

The size and the distribution of the NPs were studied using the TEM. For each set of NPs, a minimum of 100 particles were imaged to get a comprehensive view of the NPs' size distribution. The TEM images along with the particle and size distribution histograms for the 40 and 60 nm SNPs are shown in Figure 2. Moreover, the average diameters of the 40 and 60 nm sets of NPs were 41.32 ± 2.40 and 62.43 ± 3.03 nm, respectively. The standard deviations were less than 5% of the average diameters, which indicates that the particles were size homogeneous. Yet, NPs were unevenly distributed, and some clusters have been formed, which could probably alter the transmission spectrum of the NPs (Figure 2a).

Furthermore, the transmission spectra of the SNPs in their solution are shown in Figure 3a. For the 40 nm SNPs, the transmission dip occurred at 430 nm, and 93% of light was blocked at that wavelength. Moreover, the full width at half maximum

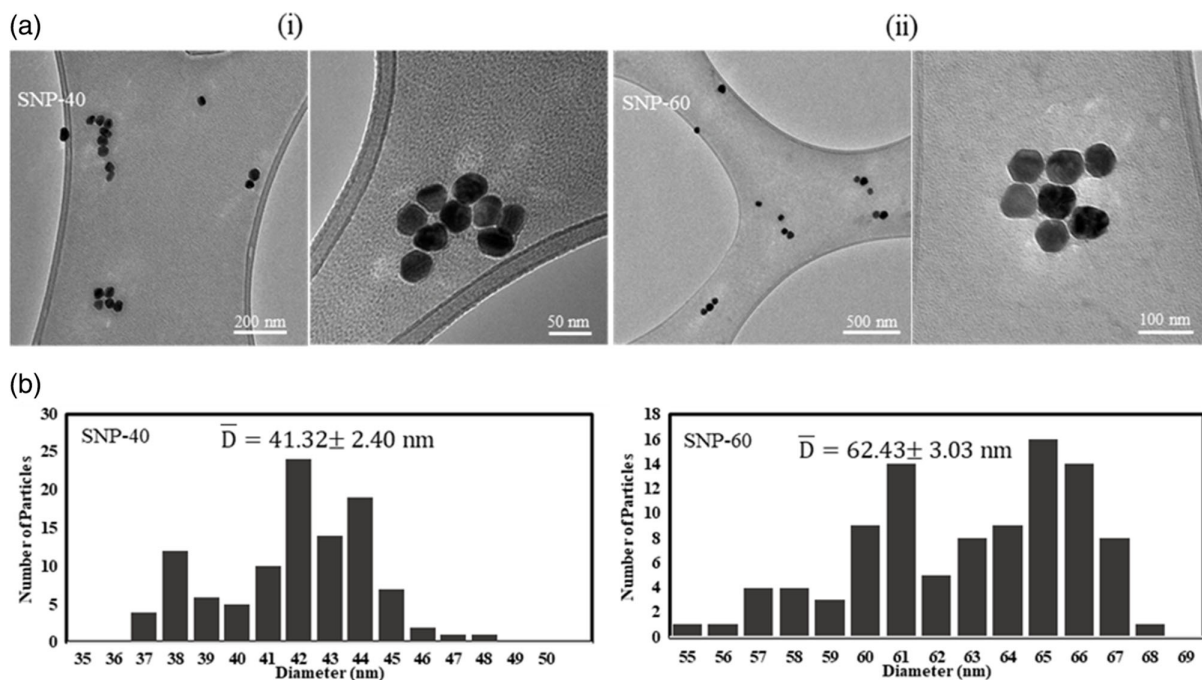


Figure 2. Morphology characterization of the SNPs. a) TEM images at different magnifications and b) size distribution histogram for the i) 40 nm and ii) 60 nm SNPs.

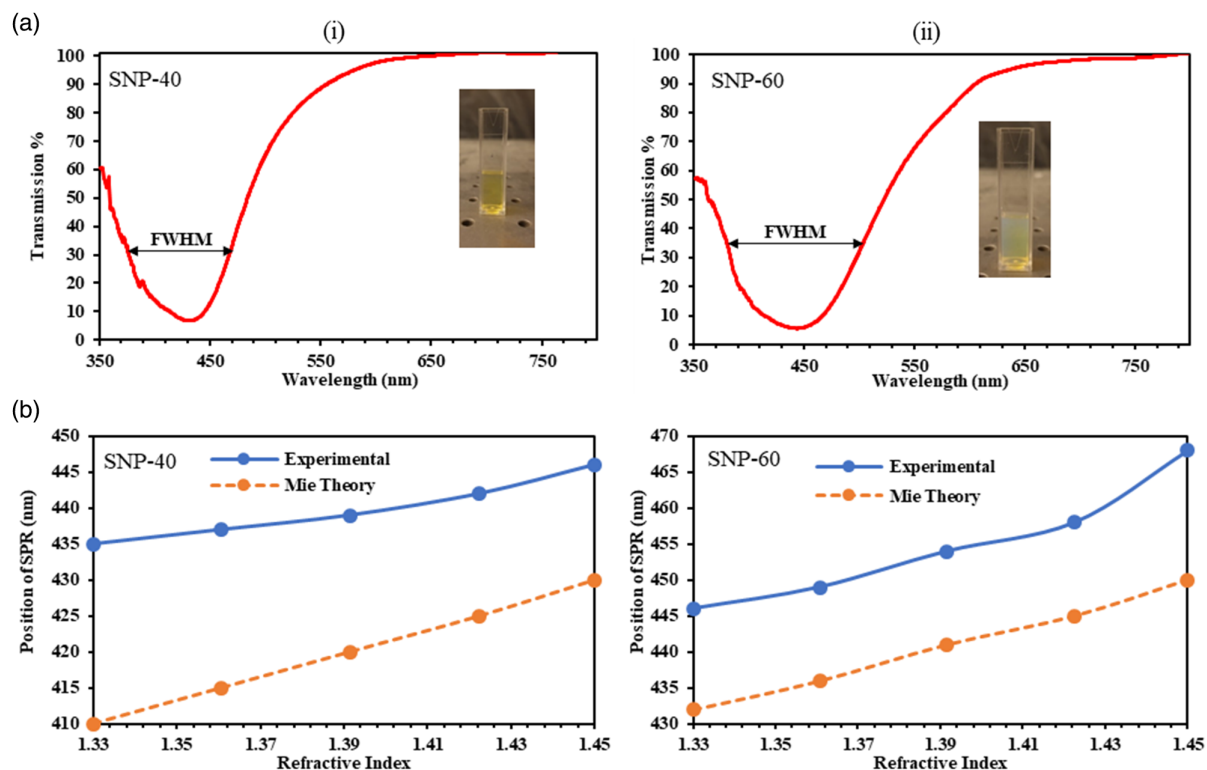


Figure 3. Prepolymerization characterization of the SNPs. a) Transmission spectrum of the solutions and b) effect of medium RI change on the surface plasmon wavelength of the i) 40 and ii) 60 nm SNPs.

(FWHM), which is a measure of the transmission bandwidth, was 93 nm (Figure 3a(i)). The transmission spectrum of the 60 SNPs showed that the SPR occurred at 442 nm, at which 94% of the light was blocked while the FWHM was 123 nm. The effect of varying the RI of the NPs solution on the SPR wavelength is demonstrated in Figure 3b. The RI characterization is essential to show how the transmission spectra of the SNP-loaded contact lenses would change if polymers other than HEMA are utilized or if HEMA was copolymerized with other materials. The experimental data were supplemented with the Mie theory predictions. In both methods, the increase in RI redshifted the position of the SPR. The experimental data and the predictions from the Mie theory were analogous in their trends with differences in the ranges of SPR shift. Garcia et al. suggest that this redshift in the NPs' spectra is due to a change in polarization of their medium; the latter causes a variation in the charge accumulation from the conduction electrons in the NPs' surface, which consequently alters the SPR properties.^[35] In fact, when embedding the NPs in a medium with a higher RI than that of water, the net charge on the NPs' surface will reduce as a result of the partial charge compensation from the new medium.^[35] Further, even though the range of variation is less than 30 nm for both NPs, the change in position of the surface plasmon suggests that light can be blocked at different wavelengths only by changing the solvent of the NPs, which is critical in CVD applications.

The prepolymerized and postpolymerized SNP-loaded contact lenses are illustrated in Figure 4a,b. The apparent color of both was trombone yellow with it being more evident at higher

concentrations (samples C–D). This was reflected in their transmission spectra shown in Figure 4c. Light blockage at the surface plasmon wavelength ranged from 43% to 75% and from 32% to 80% in the 40 and 60 nm SNP-loaded contact lenses, respectively, indicating that the intensity of the lens as a filter could easily be adjusted by varying its concentration. The SPR wavelengths of the lenses were not altered as a result of the increased NP concentration, for it remained at 446 and 469 nm for both sets, respectively. The NPs' concentration within the lens, however, altered its transparency and FWHM. As for the transparency, one can note that both SNP-loaded contact lenses (40 and 60 nm) with the lowest concentration were as expected the ones with highest transparency, at almost 78% and 90%, respectively. In addition to that, the FWHM was seen to increase with the increase in NPs' concentration; this is evident from Figure 4d(ii). Yet, in the 40 nm SNP-loaded contact lenses (Figure 4d(i)), it can be observed that the increase in concentration initially reduced the FWHM up till a certain point where the NPs' addition seemed to widen the transmission bandwidth. This signifies that there was an optimum point at which more light was blocked at the SPR without broadening the transmission dip. In Figure 4d(ii), increasing NP concentrations of the 60 nm SNP-loaded contact lenses increased the FWHM of the transmission. Further, the abrupt jump in the FWHM toward the end (75–111 nm) could be due to the excessive agglomeration of the NPs. This indicates that the transmission bandwidth, unlike the SPR position, heavily depends on the NPs' concentration.

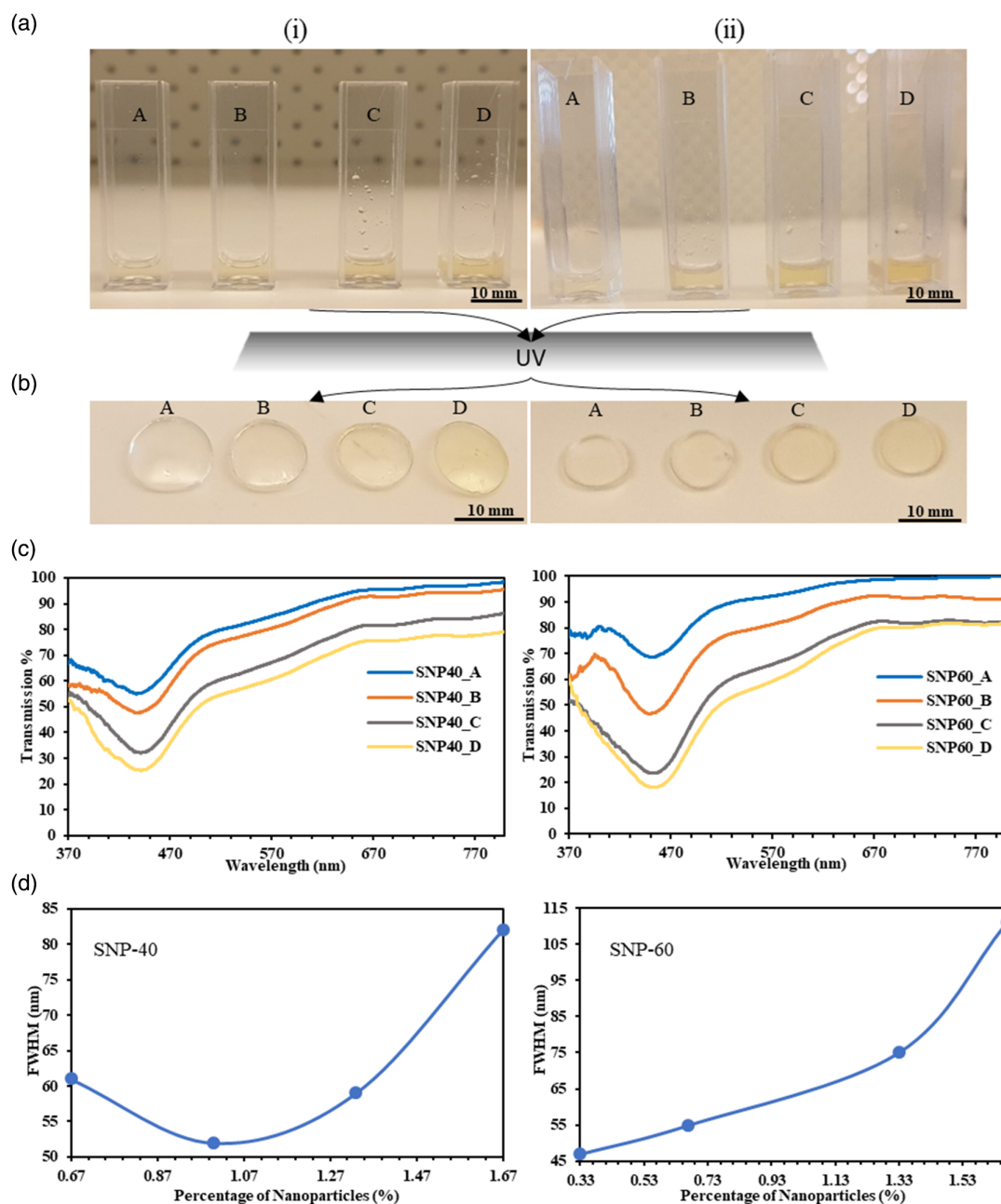


Figure 4. Polymerized i) 40 nm and ii) 60 nm SNP-loaded contact lenses at four different concentrations (A: lowest and D: highest). a) Prepolymerized nanocomposite solutions. b) Lenses postpolymerization. c) Transmission spectra of the SNP-loaded contact lenses. d) Effect of varying the NPs concentration on the FWHM of the transmission dip. Scale bar=10 mm.

The wettability and water retention of both SNP-loaded contact lens sets are shown in **Figure 5a** with images of the recorded contact angles given in **Figure 5b**. Also, cross-sectional images of the lowest and highest concentrated SNP-loaded contact lenses were studied through the SEM, and the obtained micrographs are shown in **Figure 5c**. SEM images of the lowest concentrated samples indicated that most NPs were evenly dispersed with very few formed particle clusters. It can also be seen that the number of particles was much higher than the NPs initially imaged through the TEM (**Figure 2a**), which is due to the centrifugation

of the NPs and their increased concentration. On the other hand, NPs were evidently more clustered and aggregated in highly concentrated samples. Also, those NPs were larger in size than the ones presented in **Figure 5c(A)**. For instance, the average size of the aggregates in the lowest 60 nm SNP-loaded contact lens was 126 nm while aggregates in the sample with highest concentration were composed of more than ten particles, and their average size was 1.4 μm . This explains the very steep increase in the FWHM of the highest concentrated 60 nm SNP-loaded contact lens from the one with lowest concentration (from 75 to

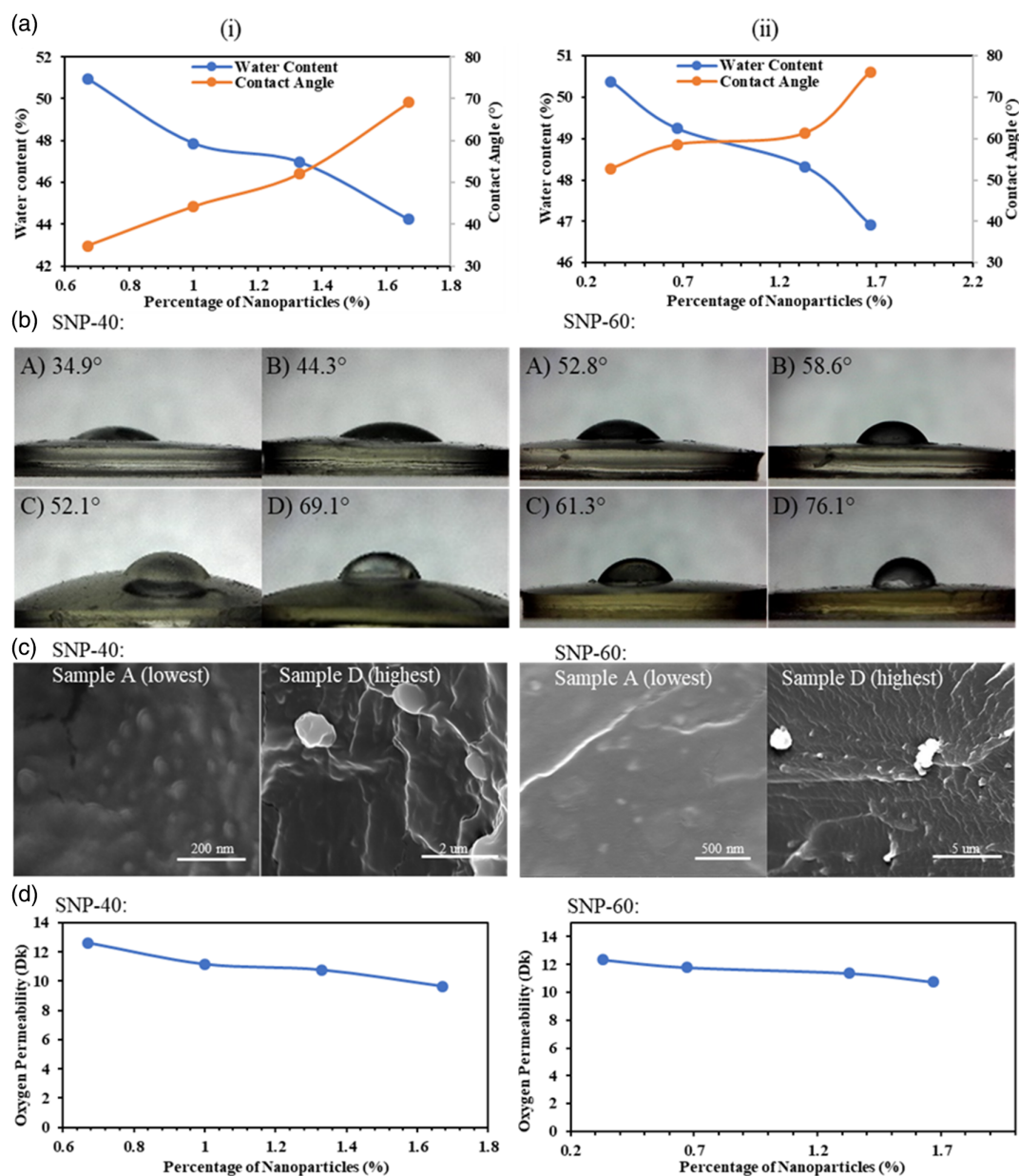


Figure 5. Postpolymerization characterization of the i) 40 and ii) 60 nm SNP-loaded contact lenses at four different concentrations (A: lowest and D: highest). a) Wettability and contact angle measurements. b) Contact angle images. c) SEM micrographs of the cross section of the lowest (A) and highest (D) concentrated samples. d) Oxygen permeability based on the empirical relation by Morgan and Efron.^[37]

111 nm). In addition, if the coalescence in both of the highest concentrated loaded contact lenses was compared (Figure 5c(D)), one can note that aggregates were comparable in size, but the effect on FWHM was much more noticeable in the case of the 60 nm SNP-loaded contact lens. This suggests that when smaller NPs aggregate, they tend to affect the transmission bandwidth less than when larger NPs agglomerate. Similar observations were previously noted utilizing gold NPs and the same hydrogel.^[36] Indeed, the excessive aggregation of the NPs in the samples was also regarded to the increased concentration resulting from NPs' centrifugation.^[36]

As predicted and shown through their transmission spectra, increasing NPs concentration in both SNP-loaded contact lenses was detrimental in their aggregation state within the lens. The interparticle coupling effects of the metallic NPs on their optical properties are well explained by Ghosh et al.^[38] Generally, when NPs aggregate, the conduction electrons in near proximity to each other (responsible for SPR illumination) become delocalized and shared among neighboring NPs; therefore, the energy required to shift the electrons decreases which, in turn, increases the wavelength at which they are activated. In the transmission spectrum, this is either represented by a slight broadening of the

transmission dip or by the complete disappearance of the surface plasmon, which occurs when NPs are in a state of total aggregation;^[38] however, this was not observed here.

Furthermore, the water retention and wettability of both SNP-loaded contact lenses decreased as a result of the increase in NPs' concentration. For the 40 nm SNP-embedded contact lenses, the 1% increase in NPs' concentration resulted in a 6.7% decrease in the swelling ratio while the same change in NPs' percentage increased the contact angle by twofold. However, the change was less pronounced in the 60 nm SNP-loaded contact lenses as the incorporation of 1.33% additional NPs decreased the water content by 3.5% and increased the contact angle by 23.3°. The increase in NPs concentration most probably formed the aggregates that were shown in Figure 5c. The formed aggregates filled up the spaces between the polymeric chains and may have reduced the effective pore size, which diminished the ability of the hydrogel to retain water effectively. Similar observations were also reported by Mollahosseini et al.^[39] who noticed a reduction in the pore size of developed membranes when SNPs were added. In fact, authors reported that SEM micrographs showed the addition of 30 and 70 nm SNPs caused a reduction in the effective pore size of the membranes. However, a decrease of less than 13% of the initial water retention value suggests that the aggregates did not severely hinder the transport within the hydrogel. Further, it can be noted that the larger sized NPs (60 nm) had a higher influence on the wettability and water content of the lenses than the smaller ones (40 nm) did, which is evident when comparing both sets of NPs at the same concentrations. For instance, at 0.67%, the water content and contact angle of the 60 nm SNP-loaded contact lens was 4% and 24° less than that of the 40 nm SNP-loaded contact lens. Moreover, similar findings, suggesting the increased surface hydrophobicity due to incorporation of larger sized NPs, were previously reported.^[39] The increase in contact angle showed that the hydrophobic SNPs were successfully integrated within the hydrogel and were present on the surface. Thus, the swelling degree lessened, and the surface of the contact lenses became more nonwetable.

Furthermore, Morgan et al.^[37] developed an exponential empirical relation between the water content and *Dk* (oxygen permeability unit), which is demonstrated below.

$$Dk = 1.67e^{0.0397EWC} \quad (8)$$

where *EWC* and *Dk* represent the equilibrium water content and oxygen permeability. Evidently, from the relation, oxygen permeability is directly proportional to water content; however, it is only applicable for conventional hydrogels that absorb oxygen through oxygen molecules in water. Utilizing the aforementioned relation, the oxygen permeability of the developed SNP-loaded contact lenses was approximated and is shown in Figure 5d. As the change in water content with NPs' concentration was insignificant, the resulting change in oxygen permeability for both sets of contact lenses was also negligible (less than two units). The oxygen permeability of the SNP-embedded contact lenses was less than that of the commercial contact lenses, which is in the range of 20–50 *Dk*, yet this could be improved by copolymerizing it with silicone hydrogels that absorb oxygen directly through their siloxane group. Incorporating HEMA with a silicone polymer

such as poly(dimethyl siloxane) (PDMS) could enhance the oxygen permeability of the contact lenses.^[40]

After characterizing them, the viability of the developed SNP-embedded contact lenses was assessed as wearables for blue-yellow CVD patients. The most optimum sample from each of the 40 and 60 nm SNP-loaded contact lenses was chosen and utilized in the analysis. These were selected based on the optical and material properties previously outlined. The effectiveness of both SNP-embedded contact lenses was first evaluated by comparing them with the spectral sensitivity of a blue-yellow patient's photoreceptor cones (Figure 6a).

Evidently, the overlapping region in the spectra between the S–M–L cones could change depending on the form and severity of the patient's CVD, yet the ideal filter should block light in the regions circled in black. The regions of overlap were at 488 and 494 nm. The transmission dip of the 40 nm SNP-loaded contact lens was 42 and 48 nm far from the mentioned intersections. The transmission dip of the 60 nm SNP-embedded contact lens was only 19 and 25 nm away from the problematic wavelengths. Nonetheless, the transmission rate of the 60 nm SNP-loaded contact lens at 485–495 nm was 34–36%, indicating that more than 60% of the incoming light was blocked. Although the transmission dip of the 60 nm SNP-embedded contact lens was significantly wide, the transmission rate was more than 60% beyond 525 nm.

In the second assessment, the transmission spectra of the two lenses were compared to that of Enchroma, which is the leading company in CVD glasses (Figure 6b). Enchroma's spectrum shows two sharp transmission dips: one at 477 nm (49% transmission) and the other at 595 nm (10% transmission rate), indicating that it can be used to aid patients affected by both forms of CVD. The first dip (at 477 nm) is what facilitates better color distinction for blue-yellow patients; hence, the other dip was not considered for this analysis. The transmission dip of both SNP-loaded contact lenses occurred at wavelengths below that of Enchroma by 31 and 8 nm, respectively. In addition, the difference in the transmission bandwidth between Enchroma and the two lenses was 21 and 23 nm, respectively.

Furthermore, in Table 1, the wettability and swelling properties of the SNP-loaded contact lenses are compared to those of the commercial lenses. The water content reported by the manufacturers was divided by the total weight and not the dry weight. Hence, the values reported in Figure 5 were adjusted to have a fair comparison. The contact angles of both developed lenses were less than those of the Acuvue lenses, and generally, the developed lenses had analogous properties to the commercial ones. Also, cytotoxicity analysis of the lenses was done using MTT reduction assay with Raw 264.7 cells as the model cells. The viability of the cells in both lenses was more than 75% after 24 h, indicating that the SNP-loaded contact lenses were indeed biocompatible (Figure 6c).

Comparing the optical properties of the developed SNP-loaded contact lenses to the gold NP-embedded lenses fabricated recently by Salih et al.,^[21] one can notice several discrepancies. Evidently, both lenses blocked light in different regions, as gold NPs instinctively absorb light in the region of 510–590 nm while SNPs' absorption ranges are 390–490 nm. The SNP-embedded contact lenses developed in this work were less selective, compared to the gold NP-loaded lenses, as they filtered out more

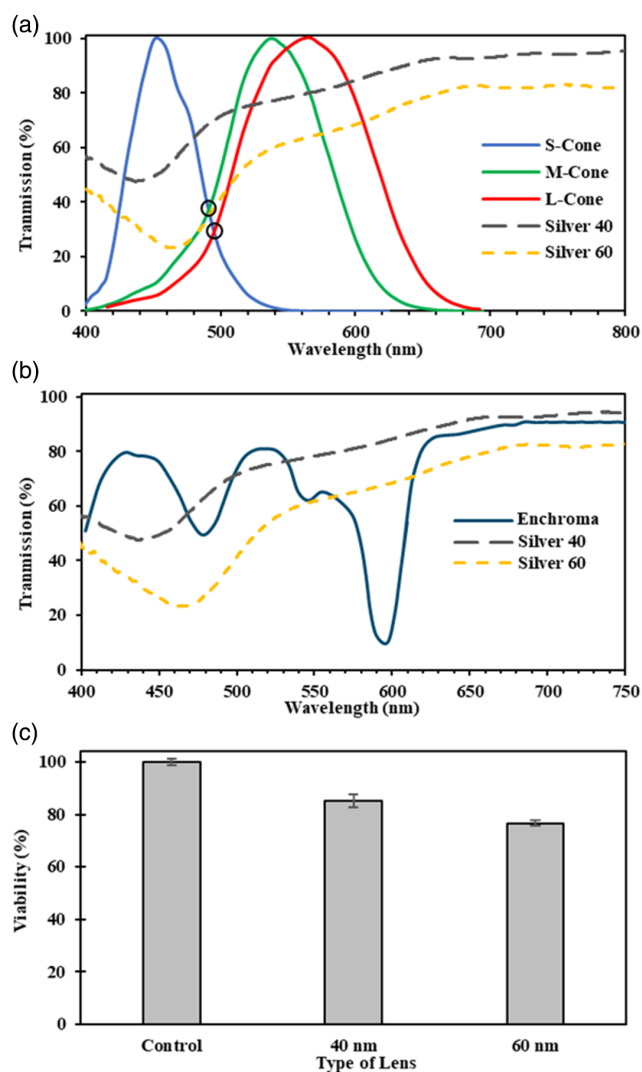


Figure 6. Performance evaluation of SNP-loaded contact lenses. a) Transmission of silver 40 and 60 nm NP-embedded contact lenses in comparison to the spectral sensitivity of a blue-yellow patient's photo-receptor cones. b) Transmission spectra of 40 and 60 nm SNP-loaded contact lenses in comparison to the spectrum of Enchroma. c) Percentage viability (biocompatibility) of the lenses after 24 h at a cell concentration of 0.0585 g mL^{-1} .

Table 1. Contact angle and water content of common commercial contact lenses^[41] and the optimum SNP-loaded contact lenses from each set.

Lens	Contact angle [°]	Water content [%]
Acuvue Advance	65.6	47.0
Acuvue Oasys	78.7	38.0
Focus Night & Day	43.9	24.0
O ₂ Optix	44.4	33.0
40 nm SNP-loaded contact lenses (this work)	52.1	32.0
60 nm SNP-loaded contact lenses (this work)	58.6	32.6

wavelengths (i.e., more of the incoming light). For instance, the FWHM of the optimum 40 nm SNP-loaded contact lens was more than that of the gold by 20 nm, which signifies a broader transmission dip. The broad transmission dip could be due to initial discrepancies in NPs' dispersion. As discussed earlier, the FWHM and the optical properties of the NPs depend significantly on the degree of their dispersion. Salih et al. reported that gold NPs were evenly distributed in the TEM micrographs,^[36] however, as shown in Figure 2, most SNPs formed clusters and were unevenly dispersed, which could have caused this anomaly in the FWHM. Nonetheless, both lenses were similar in that their water absorption capacities were not severely affected by the NPs' incorporation.

4. Conclusions

SNP-loaded contact lenses were synthesized by incorporating four different concentrations of 40 and 60 nm SNPs into HEMA-EGDMA hydrogels. As the increase in the NPs' concentration was detrimental in the lenses' wettability and transmission attributes, SNP-loaded contact lenses, which yielded optimum material and optical properties, were selected to assess their effectiveness as CVD wearable aids. In fact, the 60 nm SNP-embedded contact lenses showed that they can be used to aid blue-yellow CVD patients as they blocked more than 65% of light at the problematic wavelengths (488 and 494 nm). It also blocked light in regions near to those blocked by Enchroma, which is the current market leader for color blind glasses. Finally, the cytotoxicity analysis of the SNP-loaded contact lenses showed that they are biocompatible ($\geq 75\%$ cell viability), thus facilitating their deployment in clinical trials.

Acknowledgements

The authors acknowledge Khalifa University of Science and Technology (KUST) for the KU-KAIST Joint Research Center (Project code: 8474000220-KKJRC-2019-Health1) research funding in support on this research. H.B. and K.P. acknowledge Sandoq Al Watan LLC and Aldar Properties for the research funding (SWARD Program—AWARD, Project code: 8434000391-EX2020-044). A.K.Y. thanks the Engineering and Physical Sciences Research Council (EPSRC) for a New Investigator Award (EP/T013567/1).

Conflict of Interest

The authors declare no conflict of interest.

Data Availability Statement

The data that support the findings of this study are available from the corresponding author upon reasonable request.

Keywords

blue-yellow, color blindness, contact lenses, silver nanoparticles, wearables

Received: May 17, 2021
Revised: August 13, 2021
Published online: November 12, 2021

- [1] V. Amendola, R. Pilot, M. Frascioni, O. M. Maragò, M. A. Iatì, *J. Phys.: Condens. Matter* **2017**, *29*, 203002.
- [2] X. Huang, M. A. El-Sayed, *J. Adv. Res.* **2010**, *1*, 13.
- [3] S. Karimi, A. Moshaii, S. Abbasian, M. Nikkhal, *Plasmonics* **2019**, *14*, 851.
- [4] N. Elahi, M. Kamali, M. H. Baghersad, *Talanta* **2018**, *184*, 537.
- [5] G. Mie, *Ann. Phys.* **1908**, *330*, 377.
- [6] C. F. Bohren, D. R. Huffman, *Absorption and Scattering of Light by Small Particles*, John Wiley & Sons Weinheim, Germany **2008**.
- [7] U. Kreibig, M. Vollmer, in *Optical Properties of Metal Clusters*, Springer Berlin Heidelberg, Germany **1995**, pp. 13–201.
- [8] S. A. Maier, *Plasmonics: Fundamentals and Applications*, Springer Science & Business Media New York, US **2007**.
- [9] M. A. Garcia, *Recent Developments in Bio-Nanocomposites for Biomedical Applications*, Nova Science Publishers Hauppauge, NY, USA **2010**, p. 233.
- [10] H. A. Atwater, A. Polman, *Nat. Mater.* **2010**, *9*, 205.
- [11] W. L. Barnes, A. Dereux, T. W. Ebbesen, *Nature* **2003**, *424*, 824.
- [12] C. P. Tsangarides, A. K. Yetisen, F. da Cruz Vasconcellos, Y. Montelongo, M. M. Qasim, T. D. Wilkinson, C. R. Lowe, H. Butt, *RSC Adv.* **2014**, *4*, 10454.
- [13] A. Breuer-Weil, N. N. Almasoud, B. Abbasi, A. K. Yetisen, S.-H. Yun, H. Butt, *Nanoscale Res. Lett.* **2016**, *11*, 157.
- [14] A. K. Yetisen, H. Qu, A. Manbachi, H. Butt, M. R. Dokmeci, J. P. Hinstroza, M. Skorobogatiy, A. Khademhosseini, S. H. Yun, *ACS Nano* **2016**, *10*, 3042.
- [15] I. Prosycevas, J. Puiso, A. Guobiene, S. Tamulevičius, R. Naujokaitis, *Mater. Sci.* **2007**, *13*, 188.
- [16] R. Abargues López, P. Rodríguez Cantó, S. Albert, I. Suarez, J. Martinez-Pastor, *J. Mater. Chem. C* **2014**, *2*, 908.
- [17] J. A. Forrest, L. W. J. Jones, B. J. Hall, *Method for Altering the Optical Density and Spectral Transmission or Reflectance of Contact Lenses*, 13,883,036, **2013**.
- [18] J. Kim, E. Cha, J.-U. Park, *Adv. Mater. Technol.* **2020**, *5*, 1900728.
- [19] M. Elsherif, M. U. Hassan, A. K. Yetisen, H. Butt, *ACS Nano* **2018**, *12*, 5452.
- [20] M. Ku, J. Kim, J.-E. Won, W. Kang, Y.-G. Park, J. Park, J.-H. Lee, J. Cheon, H. H. Lee, J.-U. Park, *Sci. Adv.* **2020**, *6*, 2891.
- [21] F. Alam, M. Elsherif, B. AlQattan, A. Salih, S. M. Lee, A. K. Yetisen, S. Park, H. Butt, *ACS Biomater. Sci. Eng.* **2021**, *7*, 794.
- [22] M. P. Simunovic, *Eye* **2010**, *24*, 747.
- [23] Y.-C. Chen, Y. Guan, T. Ishikawa, H. Eto, T. Nakatsue, J. Chao, M. Ayama, *Color Res. Appl.* **2014**, *39*, 234.
- [24] J. Birch, *J. Opt. Soc. Am. A* **2012**, *29*, 313.
- [25] A. E. Salih, M. Elsherif, M. Ali, N. Vahdati, A. K. Yetisen, H. Butt, *Adv. Mater. Technol.* **2020**, *5*, 1901134.
- [26] A.-R. Badawy, M. U. Hassan, M. Elsherif, Z. Ahmed, A. K. Yetisen, H. Butt, *Adv. Healthcare Mater.* **2018**, *7*, 1800152.
- [27] M. Elsherif, A. E. Salih, A. K. Yetisen, H. Butt, *Adv. Mater. Technol.* **2021**, *6*, 2000797.
- [28] F. Alam, M. Elsherif, B. AlQattan, M. Ali, I. M. G. Ahmed, A. Salih, D. S. Antonysamy, A. K. Yetisen, S. Park, H. Butt, *Adv. Eng. Mater.* **2021**, *23*, 2000941.
- [29] R. S. Riaz, M. Elsherif, R. Moreddu, I. Rashid, M. U. Hassan, A. K. Yetisen, H. Butt, *ACS Omega* **2019**, *4*, 21792.
- [30] A. Seebeck, *Ann. Phys.* **1837**, *118*, 177.
- [31] A. W. Schmeder, D. M. McPherson, *Multi-Band Color Vision Filters and Method by Lp-Optimization*. 10,338,286, **2019**.
- [32] A. W. Schmeder, D. M. McPherson, *Multi-Band Color Vision Filters and Method by LP-Optimization*. **2019**.
- [33] S. Underwood, P. Mulvaney, *Langmuir* **1994**, *10*, 3427.
- [34] B. AlQattan, A. K. Yetisen, H. Butt, *ACS Nano* **2018**, *12*, 5130.
- [35] M. A. Garcia, *J. Phys. D: Appl. Phys.* **2011**, *44*, 283001.
- [36] A. E. Salih, M. Elsherif, F. Alam, A. K. Yetisen, H. Butt, *ACS Nano* **2021**, *15*, 4870.
- [37] P. B. Morgan, N. Efron, *Cont. Lens Anterior Eye: J. Br. Cont. Lens Assoc.* **1998**, *21*, 3.
- [38] S. K. Ghosh, T. Pal, *Chem. Rev.* **2007**, *107*, 4797.
- [39] A. Mollahosseini, A. Rahimpour, M. Jahamshahi, M. Peyravi, M. Khavarpour, *Desalination* **2012**, *306*, 41.
- [40] N. P. Tran, M. C. Yang, *Polymers* **2019**, *11*, 944.
- [41] C. Maldonado-Codina, P. B. Morgan, *J. Biomed. Mater. Res., Part A* **2007**, *83A*, 496.